Published in final edited form as:
J Proteomics. 2015 January 1; 112: 38–52. doi:10.1016/j.jprot.2014.08.007.

Comprehensive proteome quantification reveals NgBR as a new regulator for Epithelial-Mesenchymal Transition of breast tumor cells

Baofeng Zhao[1,2,#], **Bo Xu**[2,#], **Wenquan Hu**[1,#], **Chunxia Song**[2,#], **Fangjun Wang**[2], **Zhong Liu**[1], **Mingliang Ye**[2], **Hanfa Zou**[2,*], and **Qing R. Miao**[1,*]

[1]Divisions of Pediatric Surgery and Pediatric Pathology, Departments of Surgery and Pathology, Children's Research Institute, Medical College of Wisconsin, Milwaukee, WI 53226, USA

[2]Key Lab of Separation Science for Analytical Chemistry, National Chromatographic R&A Center, Dalian Institute of Chemical Physics, Chinese Academy of Sciences, Dalian, China

Abstract

Nogo-B receptor (NgBR) is a type I receptor and specifically binds to ligand Nogo-B. Our previous work has shown that NgBR is highly expressed in human breast invasive ductal carcinoma. Here, comprehensive proteome quantification was performed to examine the alteration of protein expression profile in MDA-MB-231 breast tumor cells after knocking down NgBR using lentivirus-mediated shRNA approach. Among a total of 1771 proteins feasibly quantified, 994 proteins were quantified in two biological replicates with RSD < 50%. There are 122 proteins significantly down-regulated in NgBR knockdown MDA-MB-231 breast tumor cells, such as vimentin and S100A4, well-known markers for mesenchymal cells, and CD44, a stemness indicator. The decrease of vimentin, S100A4 and CD44 protein expression levels was further confirmed by Western blot analysis. MDA-MB-231 cells are typical breast invasive ductal carcinoma cells showing mesenchymal phenotype. Cell morphology analysis demonstrates NgBR knockdown in MDA-MB-231 cells results in reversibility of Epithelial-Mesenchymal Transition (EMT), which is one of the major mechanisms involved in breast cancer metastasis. Furthermore, we demonstrated that NgBR knockdown in MCF-7 cells significantly prevented the TGF-β-induced EMT process as determined by the morphology change, and staining of E-cadherin intercellular junction as well as the decreased expression of vimentin.

[*]Corresponding authors: Qing Robert Miao, Division of Pediatric Surgery and Division of Pediatric Pathology, Department of Surgery and, Department of Pathology, Medical College of Wisconsin, Children's Research Institute, 8701, Watertown Plank Road, Milwaukee, WI 53226, USA, Tel: (414) 955-5701; Fax: (414) 955-6473; qmiao@mcw.edu. Hanfa Zou, Key Laboratory of Separation Science for Analytical Chemistry, National Chromatographic R&A Center, Dalian Institute of Chemical Physics, Chinese Academy of Sciences, 457 Zhongshan Road, Dalian 116023, China. Tel: 86-411-84379610; Fax: 86-411-84379620; hanfazou@dicp.ac.cn.
[#]B. Zhao, B. Xu, W. Hu and C. Song have equal contribution to this work.

Keywords

quantitative proteomics; Nogo-B receptor; epithelial-mesenchymal transition; breast cancer

1. Introduction

Breast cancer is one of the most frequently diagnosed cancers and the leading cause of cancer death among females [1–3]. The current combinations of early detection with screening programs and the advent of more efficacious adjuvant systemic therapy successfully decrease breast cancer mortality [4]. Such effective pathway-specific targeted and patient-tailored therapeutics requests continued advances in our understanding of the molecular biology of breast cancer progression and discovery of new prognosis markers [4]. Breast cancer is the most common malignant disease among Western women, and its metastasis of distant sites is the main cause of death [5]. Epithelial-mesenchymal transition (***EMT***) is one of major mechanisms involved in breast cancer metastasis [5–8]. During EMT, the cells lose their epithelial characteristics and acquire more migratory mesenchymal properties. EMT is a well-recognized process in embryonic development to facilitate migration of neural crest cells out of the neuroectoderm [9] [10]. EMT also happens in the formation of fibroblasts during wound healing and the transformation of epithelial cells into the invasive metastatic mesenchymal cells [9]. Here, we reveal the novel role of NgBR in promoting EMT of breast tumor cells by comprehensive proteome quantification approach.

EMT has been well documented in the progression of breast cancer [11, 12]. EMT is a complicated molecular and cellular program by which epithelial cells lose their differentiated characteristics, such as cell-cell junctions and cell polarity due to decreased expression of E-cadherin, and gain the capabilities of motility and invasiveness by acquiring mesenchymal features demonstrated by the increased expression of vimentin, a typical marker for mesenchymal cells [6–8]. Activation of TGF-β signaling pathway has been demonstrated as an important regulator for the expression of epithelial genes and induction of mesenchymal genes [6–8, 10]. In addition, cross-talk between TGF-β and PDGF, Wnt, and Notch signaling pathways also has been shown to contribute to EMT [6–8, 10]. As a downstream signaling of TGF-β, PDGF, Wnt, and Notch signaling pathways, activation of the phosphatidylinositol 3-kinase (PI3K) and Akt promotes EMT [10, 13]. Activated Akt phosphorylates glycogen synthase kinase-3β (GSK-3β) and results in inactivation of GSK-3β, which is a negative regulator for the activation of Snail that is essential signaling for EMT [13–17].

The Nogo isoforms-A, -B and -C are members of the reticulon family of proteins. Nogo-A and Nogo-C are highly expressed in the central nervous system (CNS), with Nogo-C uniquely found in skeletal muscle, while Nogo-B is found in most tissues [18, 19]. Nogo-A (also called RTN4-A) binds its specific receptors, such as NgR and LiNGO1, and acts as a negative regulator of axon sprouting [20–23]. Nogo-B was previously identified as a protein that is highly expressed in caveolin-1 enriched microdomains of endothelial cells (***EC***) [24]. The amino terminus (residues1–200) of Nogo-B (***AmNogo-B***) serves as a chemoattractant for EC [24]. Mice deficient in Nogo-A/B show exaggerated neointimal proliferation, abnormal remodeling [24] and a deficit in ischemia induced arteriogenesis and angiogenesis

[25]. NgBR was identified as a receptor specific for AmNogo-B by an expression cloning approach [26]. High affinity binding of AmNogo-B to NgBR is sufficient for AmNogo-B mediated chemotaxis and tube formation of endothelial cells [26]. We further demonstrated that NogoB-NgBR ligand-receptor pair is necessary for *in vivo* angiogenesis in zebrafish via the Akt pathway [27]. Genetic knockdown of either NogoB or NgBR by antisense morpholino abolished intersomitic vessel formation during developmental angiogenesis, and those defects can be rescued by constitutively activated Akt [27]. Our recent studies further demonstrated that NgBR is highly expressed in human breast invasive ductal carcinoma [28]. However, the exact roles of NgBR in the progression of cancer are still unclear. Here, we first utilized the on-column pseudo triplex stable isotope dimethyl labeling approach to quantify the different protein expression levels in both NgBR knockdown and control MDA-MB-231 breast cancer cells. Our results demonstrated it is an effective approach to capture the unknown biological function of NgBR from the results of global protein alteration caused by NgBR deficiency.

2. Experimental Procedures

2.1 Reagents and Materials

Polystyrene-divinylbenzene (PS-DVB) copolymer microparticles (60 μm, 300 Å) were obtained from Sepax (Suzhou, China). Daisogel ODS-AQ (3 μm, 120 Å) was purchased from DAISO Chemical CO., Ltd. (Osaka, Japan). Formic acid (FA) and sodium cyanoborohydride ($NaBH_3CN$) were provided by Fluka (Buchs, Germany). Acetonitrile (ACN, HPLC grade) was purchased from Merck (Darmstadt, Germany). Rabbit polyclonal antibodies for vimentin, CD44, E-cadherin, S100A4 and fibronectin were purchased from GeneTex, Inc. (Irvine, CA, USA). Rabbit polyclonal antibody for heat-shock protein-90 was purchased from BD Biosciences (San Jose, CA, USA). Rabbit anti-phosphorylated Akt and total Akt antibodies were purchased from Cell Signaling (Danvers, MA, USA). NgBR rabbit monoclonal antibody (Clone ID: EPR8668) was generated by Epitomics (Burlingame, CA, USA) as a collaboration project. All the other chemicals and reagents were purchased from Sigma (St. Louis, MO, USA). Fused silica capillaries with 75 and 200 μm i.d. were obtained from Polymicro Technologies (Phoenix, AZ, USA). All the water used in experiments was purified using a Milli-Q system (Millipore, Bedford, MA, USA).

2.2 Establishment of NgBR knockdown stable cell line

MDA-MB-231 cells and MCF-7 cells from ATCC (Manassas, VA, USA) were grown in DMEM (Life Technologies, Grand Island, NY, USA) containing penicillin (100 U/ml), streptomycin (100 mg/ml), and 10% (v/v) fetal calf serum (HyClone, Thermo Scientific, Pittsburgh, PA, USA). MDA-MB-231 cell were infected with lentivirus expressing non-targeting shRNAi (NS) or shRNAi targeting NgBR (shNgBR) (OpenBiosystems, Thermo Scientific, Pittsburgh, PA, USA). The sense sequence of shNgBR is 5′-CGGTCAATAAGTTGTAATCTTG-3′. Stable NS or shNgBR cell lines were established by puromycin selection. For transient knockdown experiments, MDA-MB-231 and MCF-7 cells were transfected with All-Star non-silencing siRNA (NS) or siRNA-targeting NgBR (siNgBR) (forward sequence: GGAAAUACAUAGACCUACA; reverse sequence: UGUAGGUCUAUGUAUUUCC) (QIAGEN, Valencia, CA, USA) using oligofectamine

(Life Technologies) as described before [26]. Cell morphology was observed and recorded using Nikon Eclipse TS100 microscope. At 48 h after transfection, protein and total RNA were collected for Western blot or Real-time PCR analysis (MyiQ, Bio-Rad, Hercules, CA, USA), respectively.

2.3 Sample preparation and protein digestion

Total cell lysates were prepared by adding 200 μL of cell lysis buffer (20 mM Tris-HCl (pH 7.5), 150 mM NaCl, 1 mM EDTA, 1 mM EGTA, 2.5 mM sodium pyrophosphate, 1 mM Na_3VO_4, 1 mM phenylmethylsulfonyl fluoride, 1% Triton X-100, and 1 μg/mL leupeptin) and briefly homogenized with Fisher Scientific Sonic Dismembrator Model 500. After centrifuged at 12,000 g for 30 min at 4°C, the supernatant was collected for further analysis. For proteomic analysis, proteins were precipitated with the mixture of ethanol/ether/acetic acid= 50/50/0.1 (v/v/v). The protein precipitates were collected by centrifugation at 12,000 g for 30 min at 4°C and dried by lyophilization. The pellets of protein extracts from MDA-MB-231 breast cancer cells were then dissolved in the denaturing buffer containing 8 M urea and 100 mM triethyl ammonium bicarbonate (TEAB, pH 7.6). The protein concentration was determined by Bradford assay. The proteins were reduced with dithiothreitol to the final concentration of 20 mM at 37 °C for 2 h and alkylated with iodoacetamide to the final concentration of 40 mM at room temperature in the dark for 40 min. The solution was then diluted 10-fold with 100 mM TEAB and incubated with trypsin (from bovine pancreas, TPCK treated) at the ratio of enzyme to substrate at 1/25 (w/w) at 37 °C overnight. To terminate the digestion, 1% (v/v) trifluoroacetic acid/water solution was added. All of the resulted tryptic digests were stored at −20 °C before usage.

2.4 On-column stable isotope dimethyl labeling

Firstly, the light, intermediate and heavy labeling reagents were prepared as follows: 5 mL of 50 mM sodium phosphate buffer (pH 6.8, prepared by mixing 2.5 mL of 50 mM NaH_2PO_4 with 2.5 mL of 50 mM Na_2HPO_4) is mixed with 500 μL of 4% (v/v) formaldehyde in water (CH_2O, CD_2O or $^{13}CD_2O$) and 500 μL of freshly prepared 0.6 M cyanoborohydride in water ($NaBH_3CN$ or $NaBD_3CN$). The SPE column (1 mL) with C8 plugs was packed in-house with 250 mg PS-DVB polymer-based beads (60 μm, 300 Å). Then the column was activated with 500 μL × 4 of ACN and equilibrated with 500 μL × 4 of water. Tryptic digests (200 μg in 200 μL of 100 mM TEAB solution) of NS control sample were loaded onto the SPE column and then flushed with 1 mL × 3 of the light labeling reagent. After washed by 500 μL × 2 of 50 mM sodium phosphate buffer (pH 6.8), tryptic digests (200 μg in 200 μL of 100 mM TEAB solution) of NgBR knockdown sample were loaded onto the same SPE column and then were labeled with the intermediate labeling reagent. After washed by sodium phosphate buffer, the same amount of tryptic digests of NS control sample were loaded onto the column again and labeled with the heavy labeling reagent. The labeled sample mixture was eluted with 500 μL × 2 of 80% ACN containing 5% ammonia solution and dried by the vacuum centrifugation. For biological replicate, the other batch of MDA-MB-231 breast cancer cells was prepared the same as described above.

2.5 Online two-dimensional liquid chromatography separation and mass spectrometry analysis

The HPLC system consisted of a degasser and a quaternary surveyor MS pump (Thermo Scientific, San Jose, CA, USA). 0.1% FA aqueous solution (buffer A), 0.1% FA acetonitrile solution (buffer B) and 1000 mM NH_4AC buffer (pH 2.7, buffer C) were used as the mobile phase. The separation capillary column with 75 μm i.d. was packed in-house with C18 particle (3 μm, 120 Å) to 15 cm length. For each run, the flow rate after splitting was adjusted to about 200 nL/min and a 90 min RP separation gradient was performed as follows: buffer B from 0 to 5% for 2 min, 5 to 35% for 90 min and 35 to 80% for 5 min. After flushing with 80% buffer B for 5 min, the separation system was equilibrated by buffer A for 15 min.

The automated sample injection and two-dimensional separation using the SCX-RP system were constructed as our previous report [29]. The lyophilized samples were first resuspended in 75 μL of buffer A and 25 μL of dissolved samples was injected automated onto the SCX trap column. Then, a series stepwise elution (generated by buffer A and C) with salt concentrations of 50, 100, 150, 200, 250, 300, 350, 400, 500 and 1000 mM NH_4AC (pH 2.7) was utilized to gradually elute peptides from SCX trap column to the C18 separation column. Each salt step lasted for 10 min and followed by a 15 min equilibration of buffer A. Finally, a 90 min binary RP gradient nano-RPLC MS/MS analysis as described above was applied to separate peptides prior to mass spectrometry detection in each cycle.

The LTQ-Orbitrap XL mass spectrometer (Thermo Scientific, San Jose, CA, USA) was operated in a data dependent MS/MS acquisition mode. The spray voltage was operated at 1.8 kV with the ion transfer tube at 200 °C. Full mass scan acquired in the Orbitrap mass analyzer was from *m/z* 400 to 2000 with a resolution of 60,000. Up to the 10 most intense peaks above a signal threshold of 500 were selected to fragmentation in the ion trap via collision-induced dissociation (CID). The dynamic exclusion function was set as follows: repeat count 2, repeat duration 30 s and an exclusion duration of 60 s. System controlling and data collection were carried out by Xcalibur software version 2.0.7 (Thermo Scientific).

2.6 Database searching

Raw data files were analyzed using MaxQuant (version 1.3.0.3). Spectra were searched against a NCBI human protein database (10 March 2013, 35 922 entries) downloaded from ftp://ftp.ncbi.nih.gov/refseq/H_sapiens/mRNA_Prot/human.protein.faa.gz with mass tolerance of 6 ppm and fragment mass deviation of 0.5 Da. Trypsin was set as the specific proteolytic enzyme with up to two missed cleavage sites. Carbamidomethylation (C) was searched as a fixed modification whereas oxidation (M) was searched as a variable modification. Triplets were selected as the quantification mode with the dimethyl Lys 0, 4, 8 and dimethyl N-term 0, 4, 8 selected as light, intermediate and heavy labels, respectively. The cutoff false discovery rate (FDR) at peptide level was set to 0.01. The false detection rate (FDR) was determined by equation of FDR = [2 × FP / (FP + TP)] × 100%, where FP (false positive) is the number of peptides that were identified based on sequences in the reverse database component and TP (true positive) is the number of peptides that were

identified based on sequences in the forward database component. Default settings were used for all the other parameters in MaxQuant.

2.7 Real time-PCR

Total RNA was isolated from NS or shNgBR cell lines using RNeasy kit (Qiagen). 1μg of RNA was used for RT-PCR using iScript cDNA synthesis kit (BioRad). Real-time PCR was performed with Bio-Rad MyiQ detection system (Bio-Rad, Hercules, CA, USA). Beta-actin was used as normalized control. The sequence of primers was listed in the supplemental Table S1.

2.8 Western blot analysis

Total cell extract (50 μg) was separated on a 12% SDS-PAGE gel and transferred to a nitrocellulose membrane (Bio-Rad). Protein levels were determined by using specific antibodies as described in the section of Reagents and Materials.

2.9 Immunofluorescence staining

Cells were fixed with 2% paraformaldehyde (PFA) for 10 minutes at room temperature and permeabilized with 0.1% Triton X-100 in phosphate buffered saline (pH 7.5). E-cadherin and Vimentin staining were performed using specific rabbit polyclonal primary antibodies (GeneTex) and Alex488 or Alex568 conjugated donkey anti-rabbit secondary antibodies (Life Technologies). The fluorescent images were taken by Olympus IX51 microscope.

2.10 Cell migration assay

A modified Boyden chamber was used (Costar transwell inserts; Corning Inc, Acton, MA). The transwell inserts were coated with a solution of 100 ug/ml collagen type I (BD Biosciences) in PBS at 4 °C overnight and then air-dried. MDA-MB-231 cells (5×10^4 cells) suspended in 100μl aliquot of DMEM medium containing 0.1% BSA was added to the upper chamber. After 5 hours incubation with 10%FBS DMEM medium in the bottom chamber, cells on both sides of the membrane were fixed and stained with Diff-Quik staining kit (Baxter Healthcare Corp, Dade Division, Miami, FL). The average number of cells from two randomly chosen fields (100x) on the lower side of the membrane was counted.

2.11 Statistical Analysis

Data are presented as mean ± the standard error of the mean (SEM) and the statistical significance of differences was evaluated with the ANOVA analysis. Significance was defined as $P < 0.05$.

3. Results and Discussion

3.1 Comparative proteome quantification of protein alteration in breast cancer cells with the pseudo triplex labeling approach

MDA-MB-231 cells are triple negative invasive ductal carcinoma cells originally isolated from pleural effusions of a metastatic breast cancer patient [30, 31]. To investigate the

regulatory effects of NgBR on breast tumor cell growth, we used lentivirus carrying small hairpin RNAi (shRNAi) targeting NgBR (OpenBiosystem) to establish stable NgBR knockdown MDA-MB-231 cells, and use high throughput proteomics to examine the change of protein expression profile in NgBR knockdown MDA-MB-231 cells as compared to NS control of MDA-MB-231 cells infected with non-silencing (NS) shRNAi.

For the quantitative proteome analysis, it is crucial to improve the quantification accuracy so as to correctly understand the role of protein in different physiological conditions. The common approach is to use filtering strategy to remove the spurious peptide ratio by performing multiple technical and biological replicates analyses. Statistically, multiple measurements are essential to improve the analysis accuracy. However, for large-scale proteomics analysis, multiple measurements cost many hours of precious MS time and consume more sample. Moreover, the analysis sensitivity, i.e. the number of quantified peptides, decreases significantly if multiple runs of quantitative proteomics are performed. This is because overlapped identifications among different runs of shotgun proteomics are low due to the random ion selection process in data dependent MS/MS analysis [32]. To overcome these problems in large-scale proteome quantification, a pseudo triplex labeling approach (Fig. 1) was developed in our laboratory [32]. Compared to the conventional multiple technical replicates results, the amount of quantified phosphopeptide of the novel approach increased by 50% and the experimental time reduced by 50% under the same quantification accuracy [32]. Here, it has been further testified for quantitative analysis of protein alteration happened in NgBR deficiency cells. As described in experimental section, two identical tryptic digests from the NS control of MDA-MB-231 cell lysate were labeled with the light (L) and heavy (H) labeling reagents and the third tryptic digests from NgBR knockdown MDA-MB-231 cell lysate were labeled with intermediate (M) isotope labeling reagent. In this way, two measurements of protein expression changes between NgBR knockdown and NS control groups of breast cancer cells can be achieved in one single experiment (M/L and M/H).At the same time, the ratio of heavy to light (H/L) can be served as reference system to evaluate the accuracy of quantification results. To remove the unreliable results, the quantified protein ratios in these two pseudo measurements are further filtered with the RSD between M/L and M/H < 50% (Fig. S1). By this way, a total of 4897 peptides corresponding to 1453 proteins were quantified in a 24 h on-line multidimensional separation system (Table S2). The high reliability of quantification results of comparative samples was demonstrated by the reference system with narrow distribution of log2 ratios (Fig. 2). To assure the reproducibility of the quantification results, one biological replicate was also performed and 3910 peptides corresponding to 1373 proteins were quantified (Table S3). After merging the two biological quantification results, 1771 proteins were quantified and among them 1055 proteins can be quantified in both of the biological replicated analyses. Then RSD < 50% between the two biological replicates was used as the criteria to filter the overlapped quantified proteins, which resulted in quantification of 994 proteins (Table S4). The log2 ratio distribution of the quantified proteins in both biological replicates was given in Figure 2. By achieving two-replicated analysis in one single experiment, both MS analysis time and sample amount have been significantly reduced. Meanwhile, the proteome quantification accuracy and throughput are remarkably improved.

3.2 Gene Ontology classification of the reliably quantified proteins

Among the 994 proteins quantified in both biological replicates, a threshold of 1.5-fold change was applied for the selection of proteins regulated by NgBR. It was found that 248 proteins were up-regulated whereas 122 proteins were down-regulated in the NgBR knockdown versus NS control of MDA-MB-231 breast cancer cells. Using the PANTHER (Protein Analysis Through Evolutionary Relationships) Classification System (Version 9.0, http://www.pantherdb.org), we categorized the up- and down-regulated proteins into cellular component, molecular function and biological process pertaining categories, as shown in Figure 3. For the down-regulated proteins, the cellular component (Fig. 3A) reveals that more than half of the quantified proteins in MDA-MB-231breast cancer cells were in the cell part and organelle GO category. The remaining part was associated with macromolecular complex, membrane, extracellular region, extracellular matrix and cell junction GO annotation. The molecular functional categories of the majority of proteins are binding, catalytic activity, structural molecule activity, enzyme regulator activity and transporter activity (Fig. 3B). Finally, the five most abundant classes of the biological processes that these down-regulated proteins involved in are metabolic process, cellular process, developmental process, and biological regulation (Fig. 3C). The major difference between the up- and down-regulated proteins is down-regulation of macromolecular complex and extracellular markers in GO Cellular component as shown in Figure 3A, as well as cellular component organization or biogenesis and biological adhesion in GO Biological Process as shown in Figure 3C. The list of extracellular makers and proteins related to cellular component organization and biological adhesion was summarized in Table 1. Among these proteins down-regulated in NgBR knockdown cells, several proteins have been shown to be involved in the epithelial mesenchymal transition (EMT) and stemness of breast tumor cells, such as vimentin, S100A4, smooth muscle alpha actin, and CD44 [33–36]. Vimentin, one of intermediate filament proteins, is a well-known marker for mesenchymal stem cells [33–35, 37–39]. Smooth muscle alpha actin is one of actin isoform specifically expressed in vascular smooth muscle cells and myoepithelial cells and also presented in the advanced stage of EMT [33, 36, 40]. The S100 protein family consists of 24 members and is involved in the regulation of proliferation, differentiation, apoptosis, calcium homeostasis, energy metabolism, inflammation and migration/invasion [41]. S100A4, also known as fibroblastic marker (FSP1), has been shown as a common mediator of EMT, fibrosis and regeneration [36, 42, 43]. The high mobility group A1 (HMGA1) is highly expressed during embryogenesis and in aggressive human cancer [44]. Although the role of HMGA1 in regulating EMT is not well studied, a previous report showed that HMGA1 induces the expression of Twist1, a critical transcription factor for EMT, and represses E-cadherin, a typical epithelial cell marker for intercellular junction [45]. The annexins are a super-family of closely related calcium and membrane binding proteins [46]. Annexin A1 has been shown to be increased in various cancers [46–48] and is involved in a range of cellular signal transduction pathways including cell differentiation [46, 49]. A recent report demonstrated that Annexin A1 regulates TGF-β signaling and is a candidate regulator of the EMT-like phenotypic switch during the formation of basal-like breast cancer cells [50]. Although the roles of Annexin A2 and A3 in regulating EMT are unclear, the expression of Annexin A2 and A3 is associated with poor prognosis of different types of cancer [46, 51–54]. Rab proteins are part of the large Ras superfamily of small GTPases and

regulate protein secretion, endocytosis, recycling, degradation and intracellular trafficking [55, 56]. Rab1A is highly expressed in melanoma cells and regulates membrane trafficking and exosome formation [57]. The Rab-mediated exosome signaling plays an important role in mammary gland development and cancer [58]. Rab5C promotes AMAP1-PRKD2 complex formation to enhance integrin β1 recycling in EGF-induced cancer invasion [59]. Rab11B regulates the apical recycling of the cystic fibrosis transmembrane conductance regulator (CFTR) in polarized epithelial cells [60, 61]. CD44 is a stemness indicator, and high frequency of CD44+CD24- stem cells was observed in basal-like breast tumor cells during the induction of stem cell-like cancer cells by EMT [33, 62, 63]. CD59 is a new biomarker for mesenchymal cells [64, 65]. CD151 has been shown in function during the EMT induction in hepatocellular carcinoma [66] and breast cancer cell lines [67]. MAP1B has also been reported as a biomarker for undifferentiated human bone marrow-derived mesenchymal stromal cells [68]. In addition, CDC42, Rac2 and RhoC are important members of Rho GTPase family regulating cytoskeleton formation, cell polarity, migration and tumor metastasis [69] as well as the process of EMT [70, 71]. Down-regulation of these listed proteins that are in some degree related to the EMT process, suggests that NgBR has a potential role in regulating the EMT process of breast tumor cells. Here we further validate the regulatory effects of NgBR on EMT by confirming the change of EMT biomarker expression by Western blot analysis and real-time PCR, as well as examining the transformation of epithelial cell phenotype and intercellular junction formation by immunofluorescence staining of vimentin and E-cadherin in NgBR knockdown breast tumor cells.

3.3 NgBR knockdown in MDA-MB-231 cells results in reversibility of Epithelial-Mesenchymal Transition (EMT)

MDA-MB-231 cells are mesenchymal type breast cancer cells with highly expressed mesenchymal marker vimentin and lowly expressed epithelial marker E-cadherin. The mesenchymal cell type of MDA-MB-231 cells attributes to the phenotype of highly aggressive, invasive and poorly differentiated breast cancer [72–74]. The quantitative proteomic results (Table 1) show that vimentin and S100A4, well-known markers for mesenchymal cells, and CD44, a stemness indicator, significantly decrease in NgBR knockdown MDA-MB-231 cells. The decrease of vimentin, S100A4 and CD44 protein expression levels was further confirmed by Western blot analysis as shown in Figure 4A. In addition, Western blot results (Fig. 4A) further revealed that fibronectin, which is highly expressed in mesenchymal cells but not in epithelial cells, also remarkably decreases in NgBR knockdown MDA-MB-231 cells. To further confirm if NgBR knockdown results in the mesenchymal to epithelial transition (***MET***), we determined the expression level change of several epithelial markers using real-time PCR approach. The results (Fig. 4B) demonstrate that NgBR knockdown in MDA-MB-231 cells increases the expression of epithelial markers, such as EpCAM (epithelial cell adhesion molecule), laminin-1 and nectin-1. These results suggest that NgBR knockdown promotes MET of MDA-MB-231 cells.

As shown in Figure 4C, MDA-MB-231 cells in NS control group lose their cobblestone-like epithelial appearance and present an elongated, spindle-like fibroblastic shape. Cells with

cobblestone-like epithelial cell morphology are found in NgBR knockdown MDA-MB-231 cells as pointed out with arrowheads. We found that almost all the cells are shown as spindle-like mesenchymal type cells without cell junction in NS control group, but in the NgBR knockdown group, we observed many cobblestone-like cell clusters with junctions, which are more likely to be epithelial cell morphology. In addition, the capability of cell mobility was examined by transwell migration assay as described in the Method. The results (Figure 4D) showed that NgBR knockdown decreased the mobility of MDA-MB-231 cells, which may be related to the change of epithelial cell phenotype as shown in Figure 4C.

To further confirm the specificity of NgBR knockdown by shRNAi, we used validated siRNA targeting NgBR to knock down NgBR by transient transfection approaches and then examined the effects of NgBR transient deficiency on MET of MDA-MB-231 cells. Consistent with results observed in stable cell lines as shown in Figure 4, NgBR knockdown decreased the expression of mesenchymal markers such as vimentin, fibronectin and CD44 proteins as determined by Western blot analysis (Figure S2A), and increases the epithelial cell markers such as EpCAM, laminin-1 and nectin-1 as determined by real-time PCR analysis (Figure S2B). Consequently, cells in NgBR knockdown (KD) group presented epithelial cell morphology with cobblestone-like cell clusters with junctions (Figure S2C).

As discovered by quantitative proteome analysis, vimentin and S100A4, well-known markers for mesenchymal cells, and CD44, a stemness indicator, significantly decrease in NgBR knockdown MDA-MB-231 cells. The findings suggest that NgBR knockdown changes the phenotype of MDA-MB-231 cells, which is a mesenchymal type breast tumor cells with high expression of mesenchymal marker vimentin and low expression of epithelial cell marker E-cadherin. Changes in cell phenotype between epithelial and mesenchymal states has been defined as epithelial-mesenchymal transition (EMT) and mesenchymal epithelial transition (MET), respectively [6]. The cell phenotype change process between epithelial and mesenchymal cells plays a critical role in embryonic development as well as in the pathogenesis of cancer [9, 75, 76]. It has also been shown that EMT is associated with a gain of stem cell-like behavior, which attribute to the increased metastatic process and tumor resistance [7, 8, 77–80]. During the induction of stem cell-like cancer cells by EMT, high frequency of CD44+CD24- stem cells was observed in basal-like breast tumor cells [33, 62, 63]. It is consistent with our findings (Figure 4A, Table 1) that NgBR knockdown in MDA-MB-231 cells, a basal-like breast tumor cells, diminished the mesenchymal phenotype as well as the levels of stemness marker, CD44. Epithelial cells and mesenchymal cells can been distinguished by morphology architecture and special cell markers. Epithelial cells are characterized by (1) cohesive interactions among cells to facilitate the formation of continuous cell layers; (2) existence of three membranes domains: apical, lateral and basal; (3) presence of tight junctions between apical and lateral domains; (4) apicobasal polarized distribution of the various organelles and cytoskeleton components; and (5) lack of mobility of individual epithelial cells with respect to their local environment. Different from epithelial cell architectures, mesenchymal cells have (1) loose or no interactions among cells, or no formation of continuous cell layer; (2) no clear apical and lateral membranes; (3) no apicobasal polarized distribution of organelles and cytoskeleton components; and (4) increased cell motility and invasive properties [13]. The definition of epithelial cells and mesenchymal cells is not only based on morphology, but also determined by different cell

markers. Epithelial cell markers are E-cadherin, EpCAM, Laminin-1, Nectin-1. Mesenchymal cell markers are vimentin, fibronectin, N-Cadherin, S100A4, smooth muscle alpha actin. Our results show that NgBR knockdown not only change cell morphology from an elongated, spindle-like fibroblastic shape to a cobblestone-like epithelial appearance, but also decreases the expression of mesenchymal cell markers, such as vimentin, S100A4 and fibronectin, and increases the expression of epithelial cell markers, such as EpCAM, laminin-1 and nectin-1. In addition, NgBR knockdown reduces the expression of CD44, a stemness indicator for breast cancer cells. These findings demonstrate that NgBR knockdown results in MET of MDA-MB-231 cells. It suggests that NgBR expression in tumor cells is essential for the EMT of tumor cells.

3.4 NgBR knockdown prevents the TGF-β induced EMT of MCF-7 breast tumor cells

To further demonstrate the regulatory effects of NgBR on the EMT process of breast tumor cells, we also examine the effects of NgBR knockdown on the TGF-β induced EMT process of MCF-7 cells. Unlike MDA-MB-231 basal-like breast tumor cells, MCF-7 shows the typical epithelial cell phenotype with tight junction as shown in the left panel of Figure 5A. After 48 hour of TGF-β treatment, the most of MCF-7 cells transfected with NS siRNA lost tight cell-cell junction and had a sporadic cell distribution (Fig. 5A, middle and right upper panels). However, most of NgBR knockdown MCF-7 cells with NgBR siRNA (siNgBR) still kept tight epithelial cell junction and continuous cell layers (Fig. 5A, middle and right bottom panel). Vimentin is a typical mesenchymal marker. Western blot results showed that NgBR knockdown in MCF-7 cells significantly reduced TGF-β caused vimentin expression induction as compared to NS siRNA treated MCF-7 cells (Fig. 5B). In addition, NgBR knockdown also abolished TGF-β-induced expression of ZEB1 and TWIST, which are critical transcription factors for promoting EMT procession [5–8]. To confirm the specific inhibitory effects of NgBR knockdown on TGF-β-induced EMT, we rescued the NgBR deficiency in MCF-7 cells transfected with NgBR siRNA (targeting 3'UTR region of NgBR) by transient transfection of NgBR-HA plasmid DNA (NgBR coding cDNA). As shown in Figure S3, unlike MCF-7 cells transfected with NgBR siRNA only (Fig. S3A, middle right panel), TGF-β induced the EMT procession in MCF-7/NgBR siRNA cells overexpressing NgBR-HA (Fig. S3A, bottom right panel). In addition, NgBR-HA overexpression rescued the induced expression of vimentin (Fig. S3B) and the decreased expression of E-Cadherin (Fig. S3C) in NgBR deficient MCF-7 cells. Interestingly, results of Figure S4 demonstrated that overexpression of NgBR-HA in MCF-7 cells promoted TGF-β-induced EMT procession as evidenced by the morphology change as shown in Fig. S4A and increased expression of mesenchymal maker, vimentin (Fig. S4B).

IF staining of E-cadherin, an adhesion protein presented between the cell-cell junctions of epithelial cells, further demonstrated that E-cadherin presents at the cell-cell junction of MCF-7 cells before the TGF-β treatment (Fig. 6A, upper panels). TGF-β treatment results in the loss of E-cadherin presented at the cell-cell junction of MCF-7 cells infected with NS siRNA (Fig. 6A, left bottom panel). However, E-cadherin staining between cell-cell junctions still can be detected in MCF-7 cells infected with NgBR siRNA (Fig. 6A, right bottom panel). Opposite to E-cadherin staining, vimentin staining only can be detected in TGF-β treated NS MCF-7 cells (Fig. 6B, left bottom panel), but not in NS MCF-7 cells

without TGF-β treatment (Fig. 6B, left upper panel) or NgBR knockdown MCF-7 cells treated with or without TGF-β (Fig. 6B, right bottom and upper panels, respectively). It clearly demonstrated that TGF–β induced EMT transition of MCF-7 cells and NgBR knockdown prevented the EMT transition. Combined with MDA-MB-231 results, it reveals that NgBR is not only required for keeping mesenchymal phenotype of MDA-MB-231 malignant breast tumor cells, but also is essential for TGF-β induced EMT procession of MCF-7 benign breast tumor cells. As shown in Figure S4C, expression levels of both Nogo-B and NgBR in MDA-MB-231 cells are much higher than in MCF-7, which may interpret the mesenchymal phenotype presented in MDA-MB-231 cells.

3.5 NgBR knockdown impairs the activation of Akt in breast tumor cells

Given these findings, we sought to determine the molecular mechanism by which NgBR regulates the switch of EMT and MET. It has been shown that TGF-β, and Wnt/β-catenin signaling as well as hypoxia triggers EMT activation [6, 10, 13, 81, 82]. However, PI3K/Akt axis is required for all of these signaling-mediated EMT [13, 83-86]. It has been demonstrated that PI3K inhibitor LY294002 and dominant-negative Akt mutants block the TGF-β-induced EMT [13, 87, 88]. Therefore, we examined the change of Akt activation in NgBR knockdown MDA-MB-231 cells by determining the phosphorylation of Akt using Western blot analysis. The results (Fig. 7A/B) show that NgBR knockdown in MDA-MB-231 cells significantly abolishes the phosphorylation of Akt when compared to control cells. However, total protein levels of Akt in NgBR knockdown cells did not change when compared to control cells. It suggests that NgBR knockdown only impairs the activation of Akt in MDA-MB-231 cells. Similarly, NgBR knockdown also diminished the TGF-β stimulated phosphorylation of Akt but not reduced the total Akt protein levels in MCF-7 when compared to control cells (Fig. 7C/D). In summary, our results show that NgBR knockdown reduces the TGF-β-stimulated phosphorylation of Akt in breast tumor cells, which may contribute to inhibition of EMT. The regulatory effects of NgBR on the VEGF-stimulated phosphorylation of Akt in endothelial cells also have been demonstrated in our previous report [24, 26, 27]. However, the molecular mechanism by which NgBR regulates the Akt phosphorylation needs further investigation.

Although Nogo-B and NgBR have been demonstrated to play the important roles in regulating endothelial cell migration and blood vessel formation [24, 26, 27], roles of Nogo-B and NgBR in cancer cells and cancer progression are still unclear. Nogo-B (also named as ASY) was previously identified as one of apoptosis-inducing genes to human cancer [89]. Ectopic expression of the Nogo-B/ASY gene led to extensive apoptosis, particularly in cancer cells [89]. They further demonstrated that Nogo-B/ASY overexpression contributes to endoplasmic reticulum stress and induces apoptosis through Ca^{2+} depletion in endoplasmic reticulum [90]. However, at the same time, stable transfectants overexpressing high levels of Nogo-B/ASY are resistant to endoplasmic reticulum stress associated stimuli, which implies that Nogo-B/ASY overexpression activates protective response to endoplasmic reticulum stress [90]. In addition, the osteosarcoma SaOS-2 cell lines and the CHO cell lines do express high levels of endogenous Nogo-B. Overexpression of Nogo-B in both SaOS-2 and CHO cell lines do not differ significantly from the respective parental wild-type or control cell lines both in respect to cell proliferation and to spontaneous

apoptosis or cell death induced by staurosporine and tunicamycin [91]. These controversial studies cause the uncertainty about the precise roles of Nogo-B in modulating the apoptosis of cancer cells. Our preliminary results show that overexpression of amino-terminal domain of Nogo-B (AmNogo-B) does not cause any significant effects on tumor cell growth and cell survival (data not shown). Knockdown of NgBR also does not significantly affect the growth and survival of MCF-7 cells under basal growth condition [28]. The detailed roles of NgBR in breast cancer really need further investigation.

4. Conclusion

This is the first study to use quantitative proteomics analysis to investigate the global role of NgBR in regulating breast cancer cells. The findings from this study demonstrate: (a) the on-column pseudo triplex labeling approach improves the quantification accuracy and throughput of the large-scale comparative proteomics analysis; (b) NgBR knockdown diminishes the expression of mesenchymal cell markers and increases the expression of epithelial cell markers; (c) NgBR knockdown results in MET of MDA-MB-231 cells; (d) as a proof of concept, NgBR knockdown also prevents the TGF-β induced EMT of MCF-7 cells, and finally, (e) NgBR is also required for activation of Akt kinase in both MDA-MB-231 cells and MCF-7 cells, which are central signaling for EMT. These results suggest that NgBR-mediated Akt activation may play an important role in switching decision between EMT and MET.

In summary, this study provides a good example to demonstrate that quantitative proteomics analysis provides biologists with a powerful tool to explore unknown biological function. The EMT has been implicated in two of the most important processes responsible for cancer-related mortality: progression to distant metastatic diseases and acquisition of therapeutic resistance [6–8]. The findings of this study demonstrate NgBR is a potential regulator for breast tumor metastasis and tumor resistance because NgBR knockdown blocks EMT. Therefore, NgBR may be a novel therapeutic target for breast cancer.

Supplementary Material

Refer to Web version on PubMed Central for supplementary material.

Acknowledgments

This work is supported in part by start-up funds from Division of Pediatric Surgery and Division of Pediatric Pathology, Medical College of Wisconsin (MCW) and Advancing a Healthier Wisconsin endowment to MCW, NIH/NHLBI R01HL108938, Wisconsin Breast Cancer Showhouse (WBCS), ACS and MCW Cancer Center pilot grant, and State of Wisconsin Tax Check-off program for breast & prostate cancer research to Q.R.M., and AHA postdoctoral fellowship to B.Z, and the Creative Research Group Project of NSFC (21021004), the China State Key Basic Research Program Grant (2013CB911202, 2012CB910101, 2012CB910604) to H.Z..

Abbreviations

NgBR	Nogo-B receptor
EMT	Epithelial-Mesenchymal Transition

PI3K	phosphatidylinositol 3-kinase
GSK-3β	glycogen synthase kinase-3β
CNS	central nervous system
EC	endothelial cells
AmNogo-B	amino-terminal domain of Nogo-B
PS-DVB	polystyrene-divinylbenzene
FA	formic acid
$NaBH_3CN$	sodium cyanoborohydride
ACN	acetonitrile
NS	non-silencing
shNgBR	shRNAi/siRNA, shRNAi targeting NgBR
siNgBR	siRNA-targeting NgBR
NaCl	sodium chloride
EDTA	ethylene diamine tetraacetic acid
EGTA	ethylene glycol tetraacetic acid
Na_3VO_4	sodium orthovanadate
TEAB	triethyl ammonium bicarbonate
NaH_2PO_4	monosodium phosphate
Na_2HPO_4	disodium phosphate
SPE	solid-phase extraction
HPLC	high-performance liquid chromatography
MS	mass spectrometry
RP	reverse phase
SCX	strong cation exchange
CID	collision-induced dissociation
FDR	false detection rate
FP	false positive
TP	true positive
SDS-PAGE	sodium dodecyl sulfate polyacrylamide gel electrophoresis
PFA	paraformaldehyde
SEM	standard error of the mean
H/L	heavy/light

M/L	intermediate/light
M/H	intermediate/heavy
RSD	relative standard deviation
GO	gene ontology
PANTHER	protein analysis through evolutionary relationships
FSP1	fibroblastic marker
HMGA1	high mobility group A1
CFTR	cystic fibrosis transmembrane conductance regulator
MET	mesenchymal to epithelial transition
EpCAM	epithelial cell adhesion molecule

References

1. Jemal A, Bray F, Center MM, Ferlay J, Ward E, Forman D. Global cancer statistics. CA: a cancer journal for clinicians. 2011; 61:69–90. [PubMed: 21296855]
2. DeSantis C, Siegel R, Bandi P, Jemal A. Breast cancer statistics, 2011. CA: a cancer journal for clinicians. 2011; 61:409–18. [PubMed: 21969133]
3. Siegel R, Naishadham D, Jemal A. Cancer statistics, 2012. CA: a cancer journal for clinicians. 2012; 62:10–29. [PubMed: 22237781]
4. Bombonati A, Sgroi DC. The molecular pathology of breast cancer progression. The Journal of pathology. 2011; 223:307–17. [PubMed: 21125683]
5. Weigelt B, Peterse JL, van ‘t Veer LJ. Breast cancer metastasis: markers and models. Nature reviews. 2005; 5:591–602.
6. Polyak K, Weinberg RA. Transitions between epithelial and mesenchymal states: acquisition of malignant and stem cell traits. Nature reviews. 2009; 9:265–73.
7. Brabletz T. EMT and MET in Metastasis: Where Are the Cancer Stem Cells? Cancer Cell. 2012; 22:699–701. [PubMed: 23238008]
8. Brabletz T. To differentiate or not--routes towards metastasis. Nature reviews. 2012; 12:425–36.
9. Yang J, Weinberg RA. Epithelial-mesenchymal transition: at the crossroads of development and tumor metastasis. Developmental cell. 2008; 14:818–29. [PubMed: 18539112]
10. Jo M, Lester RD, Montel V, Eastman B, Takimoto S, Gonias SL. Reversibility of epithelial-mesenchymal transition (EMT) induced in breast cancer cells by activation of urokinase receptor-dependent cell signaling. The Journal of biological chemistry. 2009; 284:22825–33. [PubMed: 19546228]
11. Mani SA, Guo W, Liao MJ, Eaton EN, Ayyanan A, Zhou AY, et al. The epithelial-mesenchymal transition generates cells with properties of stem cells. Cell. 2008; 133:704–15. [PubMed: 18485877]
12. Morel AP, Lievre M, Thomas C, Hinkal G, Ansieau S, Puisieux A. Generation of breast cancer stem cells through epithelial-mesenchymal transition. PLoS One. 2008; 3:e2888. [PubMed: 18682804]
13. Larue L, Bellacosa A. Epithelial-mesenchymal transition in development and cancer: role of phosphatidylinositol 3’ kinase/AKT pathways. Oncogene. 2005; 24:7443–54. [PubMed: 16288291]
14. Bachelder RE, Yoon SO, Franci C, de Herreros AG, Mercurio AM. Glycogen synthase kinase-3 is an endogenous inhibitor of Snail transcription: implications for the epithelial-mesenchymal transition. J Cell Biol. 2005; 168:29–33. [PubMed: 15631989]

15. Zhou BP, Deng J, Xia W, Xu J, Li YM, Gunduz M, et al. Dual regulation of Snail by GSK-3beta-mediated phosphorylation in control of epithelial-mesenchymal transition. Nature cell biology. 2004; 6:931–40.
16. Batlle E, Sancho E, Franci C, Dominguez D, Monfar M, Baulida J, et al. The transcription factor snail is a repressor of E-cadherin gene expression in epithelial tumour cells. Nature cell biology. 2000; 2:84–9.
17. Cano A, Perez-Moreno MA, Rodrigo I, Locascio A, Blanco MJ, del Barrio MG, et al. The transcription factor snail controls epithelial-mesenchymal transitions by repressing E-cadherin expression. Nature cell biology. 2000; 2:76–83.
18. Huber AB, Weinmann O, Brosamle C, Oertle T, Schwab ME. Patterns of Nogo mRNA and protein expression in the developing and adult rat and after CNS lesions. J Neurosci. 2002; 22:3553–67. [PubMed: 11978832]
19. Josephson A, Trifunovski A, Widmer HR, Widenfalk J, Olson L, Spenger C. Nogo-receptor gene activity: cellular localization and developmental regulation of mRNA in mice and humans. The Journal of comparative neurology. 2002; 453:292–304. [PubMed: 12378589]
20. Chen MS, Huber AB, van der Haar ME, Frank M, Schnell L, Spillmann AA, et al. Nogo-A is a myelin-associated neurite outgrowth inhibitor and an antigen for monoclonal antibody IN-1. Nature. 2000; 403:434–9. [PubMed: 10667796]
21. Reilly CE. Nogo-A is the inhibitor of CNS axon regeneration. Journal of neurology. 2000; 247:239–40. [PubMed: 10787127]
22. Grandpre T, Strittmatter SM. Nogo: a molecular determinant of axonal growth and regeneration. Neuroscientist. 2001; 7:377–86. [PubMed: 11597097]
23. Oertle T, Schwab ME. Nogo and its paRTNers. Trends Cell Biol. 2003; 13:187–94. [PubMed: 12667756]
24. Acevedo L, Yu J, Erdjument-Bromage H, Miao RQ, Kim JE, Fulton D, et al. A new role for Nogo as a regulator of vascular remodeling. Nature medicine. 2004; 10:382–8.
25. Yu J, Fernandez-Hernando C, Suarez Y, Schleicher M, Hao Z, Wright PL, et al. Reticulon 4B (Nogo-B) is necessary for macrophage infiltration and tissue repair. Proceedings of the National Academy of Sciences of the United States of America. 2009; 106:17511–6. [PubMed: 19805174]
26. Miao RQ, Gao Y, Harrison KD, Prendergast J, Acevedo LM, Yu J, et al. Identification of a receptor necessary for Nogo-B stimulated chemotaxis and morphogenesis of endothelial cells. Proceedings of the National Academy of Sciences of the United States of America. 2006; 103:10997–1002. [PubMed: 16835300]
27. Zhao B, Chun C, Liu Z, Horswill MA, Pramanik K, Wilkinson GA, et al. Nogo-B receptor is essential for angiogenesis in zebrafish via Akt pathway. Blood. 2010; 116:5423–33. [PubMed: 20813898]
28. Wang B, Zhao B, North PE, Kong A, Huang J, Miao QR. Expression of NgBR is highly associated with estrogen receptor alpha and survivin in breast cancer. PLoS One. 2013; 8(11):e78083. [PubMed: 24223763]
29. Wang F, Dong J, Jiang X, Ye M, Zou H. Capillary trap column with strong cation-exchange monolith for automated shotgun proteome analysis. Analytical chemistry. 2007; 79:6599–606. [PubMed: 17676922]
30. Cailleau R, Mackay B, Young RK, Reeves WJ Jr. Tissue culture studies on pleural effusions from breast carcinoma patients. Cancer research. 1974; 34:801–9. [PubMed: 4592574]
31. Cailleau R, Young R, Olive M, Reeves WJ Jr. Breast tumor cell lines from pleural effusions. J Natl Cancer Inst. 1974; 53:661–74. [PubMed: 4412247]
32. Song C, Wang F, Ye M, Cheng K, Chen R, Zhu J, et al. Improvement of the quantification accuracy and throughput for phosphoproteome analysis by a pseudo triplex stable isotope dimethyl labeling approach. Analytical chemistry. 2011; 83:7755–62. [PubMed: 21902226]
33. Sarrio D, Rodriguez-Pinilla SM, Hardisson D, Cano A, Moreno-Bueno G, Palacios J. Epithelial-mesenchymal transition in breast cancer relates to the basal-like phenotype. Cancer research. 2008; 68:989–97. [PubMed: 18281472]

34. Lee K, Nelson CM. New insights into the regulation of epithelial-mesenchymal transition and tissue fibrosis. International review of cell and molecular biology. 2012; 294:171–221. [PubMed: 22364874]
35. Scanlon CS, Van Tubergen EA, Inglehart RC, D'Silva NJ. Biomarkers of epithelial-mesenchymal transition in squamous cell carcinoma. Journal of dental research. 2013; 92:114–21. [PubMed: 23128109]
36. Guarino M, Tosoni A, Nebuloni M. Direct contribution of epithelium to organ fibrosis: epithelial-mesenchymal transition. Human pathology. 2009; 40:1365–76. [PubMed: 19695676]
37. Kokkinos MI, Wafai R, Wong MK, Newgreen DF, Thompson EW, Waltham M. Vimentin and epithelial-mesenchymal transition in human breast cancer--observations in vitro and in vivo. Cells, tissues, organs. 2007; 185:191–203. [PubMed: 17587825]
38. Heatley M, Whiteside C, Maxwell P, Toner P. Vimentin expression in benign and malignant breast epithelium. Journal of clinical pathology. 1993; 46:441–5. [PubMed: 7686566]
39. Hu L, Lau SH, Tzang CH, Wen JM, Wang W, Xie D, et al. Association of Vimentin overexpression and hepatocellular carcinoma metastasis. Oncogene. 2004; 23:298–302. [PubMed: 14647434]
40. Masszi A, Di Ciano C, Sirokmany G, Arthur WT, Rotstein OD, Wang J, et al. Central role for Rho in TGF-beta1-induced alpha-smooth muscle actin expression during epithelial-mesenchymal transition. American journal of physiology Renal physiology. 2003; 284:F911–24. [PubMed: 12505862]
41. Donato R, Cannon BR, Sorci G, Riuzzi F, Hsu K, Weber DJ, et al. Functions of S100 proteins. Current molecular medicine. 2013; 13:24–57. [PubMed: 22834835]
42. Schneider M, Hansen JL, Sheikh SP. S100A4: a common mediator of epithelial-mesenchymal transition, fibrosis and regeneration in diseases? J Mol Med (Berl). 2008; 86:507–22. [PubMed: 18322670]
43. Kalluri R, Neilson EG. Epithelial-mesenchymal transition and its implications for fibrosis. The Journal of clinical investigation. 2003; 112:1776–84. [PubMed: 14679171]
44. Shah SN, Resar LM. High mobility group A1 and cancer: potential biomarker and therapeutic target. Histology and histopathology. 2012; 27:567–79. [PubMed: 22419021]
45. Belton A, Gabrovsky A, Bae YK, Reeves R, Iacobuzio-Donahue C, Huso DL, et al. HMGA1 induces intestinal polyposis in transgenic mice and drives tumor progression and stem cell properties in colon cancer cells. PLoS One. 2012; 7:e30034. [PubMed: 22276142]
46. Mussunoor S, Murray GI. The role of annexins in tumour development and progression. The Journal of pathology. 2008; 216:131–40. [PubMed: 18698663]
47. Wang Y, Serfass L, Roy MO, Wong J, Bonneau AM, Georges E. Annexin-I expression modulates drug resistance in tumor cells. Biochemical and biophysical research communications. 2004; 314:565–70. [PubMed: 14733945]
48. Zimmermann U, Woenckhaus C, Teller S, Venz S, Langheinrich M, Protzel C, et al. Expression of annexin AI in conventional renal cell carcinoma (CRCC) correlates with tumour stage, Fuhrman grade, amount of eosinophilic cells and clinical outcome. Histology and histopathology. 2007; 22:527–34. [PubMed: 17330807]
49. Lim LH, Pervaiz S. Annexin 1: the new face of an old molecule. Faseb J. 2007; 21:968–75. [PubMed: 17215481]
50. de Graauw M, van Miltenburg MH, Schmidt MK, Pont C, Lalai R, Kartopawiro J, et al. Annexin A1 regulates TGF-beta signaling and promotes metastasis formation of basal-like breast cancer cells. Proceedings of the National Academy of Sciences of the United States of America. 2010; 107:6340–5. [PubMed: 20308542]
51. Emoto K, Sawada H, Yamada Y, Fujimoto H, Takahama Y, Ueno M, et al. Annexin II overexpression is correlated with poor prognosis in human gastric carcinoma. Anticancer research. 2001; 21:1339–45. [PubMed: 11396210]
52. Emoto K, Yamada Y, Sawada H, Fujimoto H, Ueno M, Takayama T, et al. Annexin II overexpression correlates with stromal tenascin-C overexpression: a prognostic marker in colorectal carcinoma. Cancer. 2001; 92:1419–26. [PubMed: 11745218]

53. Deng S, Wang J, Hou L, Li J, Chen G, Jing B, et al. Annexin A1, A2, A4 and A5 play important roles in breast cancer, pancreatic cancer and laryngeal carcinoma, alone and/or synergistically. Oncology letters. 2013; 5:107–12. [PubMed: 23255903]
54. Wu N, Liu S, Guo C, Hou Z, Sun MZ. The role of annexin A3 playing in cancers. Clin Transl Oncol. 2013; 15:106–10. [PubMed: 23011854]
55. Recchi C, Seabra MC. Novel functions for Rab GTPases in multiple aspects of tumour progression. Biochemical Society transactions. 2012; 40:1398–403. [PubMed: 23176488]
56. Kelly EE, Horgan CP, Goud B, McCaffrey MW. The Rab family of proteins: 25 years on. Biochemical Society transactions. 2012; 40:1337–47. [PubMed: 23176478]
57. Peinado H, Aleckovic M, Lavotshkin S, Matei I, Costa-Silva B, Moreno-Bueno G, et al. Melanoma exosomes educate bone marrow progenitor cells toward a pro-metastatic phenotype through MET. Nature medicine. 2012; 18:883–91.
58. Hendrix A, Hume AN. Exosome signaling in mammary gland development and cancer. The International journal of developmental biology. 2011; 55:879–87. [PubMed: 22161843]
59. Onodera Y, Nam JM, Hashimoto A, Norman JC, Shirato H, Hashimoto S, et al. Rab5c promotes AMAP1-PRKD2 complex formation to enhance beta1 integrin recycling in EGF-induced cancer invasion. J Cell Biol. 2012; 197:983–96. [PubMed: 22734003]
60. Silvis MR, Bertrand CA, Ameen N, Golin-Bisello F, Butterworth MB, Frizzell RA, et al. Rab11b regulates the apical recycling of the cystic fibrosis transmembrane conductance regulator in polarized intestinal epithelial cells. Molecular biology of the cell. 2009; 20:2337–50. [PubMed: 19244346]
61. Kelly EE, Horgan CP, McCaffrey MW. Rab11 proteins in health and disease. Biochemical Society transactions. 2012; 40:1360–7. [PubMed: 23176481]
62. Mani SA, Yang J, Brooks M, Schwaninger G, Zhou A, Miura N, et al. Mesenchyme Forkhead 1 (FOXC2) plays a key role in metastasis and is associated with aggressive basal-like breast cancers. Proceedings of the National Academy of Sciences of the United States of America. 2007; 104:10069–74. [PubMed: 17537911]
63. Honeth G, Bendahl PO, Ringner M, Saal LH, Gruvberger-Saal SK, Lovgren K, et al. The CD44+/CD24- phenotype is enriched in basal-like breast tumors. Breast Cancer Res. 2008; 10:R53. [PubMed: 18559090]
64. Komoda H, Okura H, Lee CM, Sougawa N, Iwayama T, Hashikawa T, et al. Reduction of N-glycolylneuraminic acid xenoantigen on human adipose tissue-derived stromal cells/mesenchymal stem cells leads to safer and more useful cell sources for various stem cell therapies. Tissue engineering Part A. 2010; 16:1143–55. [PubMed: 19863253]
65. Fust A, Pallinger E, Stundl A, Kovacs E, Imre L, Toth S, et al. Both freshly prepared and frozen-stored amniotic membrane cells express the complement inhibitor CD59. TheScientificWorldJournal. 2012; 2012:815615.
66. Ke AW, Shi GM, Zhou J, Huang XY, Shi YH, Ding ZB, et al. CD151 amplifies signaling by integrin alpha6beta1 to PI3K and induces the epithelial-mesenchymal transition in HCC cells. Gastroenterology. 2011; 140:1629–41. e15. [PubMed: 21320503]
67. Arora H, Qureshi R, Park WY. miR-506 regulates epithelial mesenchymal transition in breast cancer cell lines. PLoS One. 2013; 8:e64273. [PubMed: 23717581]
68. Montzka K, Lassonczyk N, Tschoke B, Neuss S, Fuhrmann T, Franzen R, et al. Neural differentiation potential of human bone marrow-derived mesenchymal stromal cells: misleading marker gene expression. BMC neuroscience. 2009; 10:16. [PubMed: 19257891]
69. Karlsson R, Pedersen ED, Wang Z, Brakebusch C. Rho GTPase function in tumorigenesis. Biochim Biophys Acta. 2009; 1796:91–8. [PubMed: 19327386]
70. Hutchison N, Hendry BM, Sharpe CC. Rho isoforms have distinct and specific functions in the process of epithelial to mesenchymal transition in renal proximal tubular cells. Cell Signal. 2009; 21:1522–31. [PubMed: 19477269]
71. Bendris N, Arsic N, Lemmers B, Blanchard JM. Cyclin A2, Rho GTPases and EMT. Small GTPases. 2012; 3:225–8. [PubMed: 22735340]

72. Lacroix M, Haibe-Kains B, Hennuy B, Laes JF, Lallemand F, Gonze I, et al. Gene regulation by phorbol 12-myristate 13-acetate in MCF-7 and MDA-MB-231, two breast cancer cell lines exhibiting highly different phenotypes. Oncol Rep. 2004; 12:701–7. [PubMed: 15375488]
73. Charafe-Jauffret E, Ginestier C, Monville F, Finetti P, Adelaide J, Cervera N, et al. Gene expression profiling of breast cell lines identifies potential new basal markers. Oncogene. 2006; 25:2273–84. [PubMed: 16288205]
74. Lacroix M, Leclercq G. Relevance of breast cancer cell lines as models for breast tumours: an update. Breast Cancer Res Treat. 2004; 83:249–89. [PubMed: 14758095]
75. Baum B, Settleman J, Quinlan MP. Transitions between epithelial and mesenchymal states in development and disease. Seminars in cell & developmental biology. 2008; 19:294–308. [PubMed: 18343170]
76. Hugo H, Ackland ML, Blick T, Lawrence MG, Clements JA, Williams ED, et al. Epithelial--mesenchymal and mesenchymal--epithelial transitions in carcinoma progression. Journal of cellular physiology. 2007; 213:374–83. [PubMed: 17680632]
77. Yu F, Yao H, Zhu P, Zhang X, Pan Q, Gong C, et al. let-7 regulates self renewal and tumorigenicity of breast cancer cells. Cell. 2007; 131:1109–23. [PubMed: 18083101]
78. Robson EJ, Khaled WT, Abell K, Watson CJ. Epithelial-to-mesenchymal transition confers resistance to apoptosis in three murine mammary epithelial cell lines. Differentiation; research in biological diversity. 2006; 74:254–64.
79. Kang Y, Massague J. Epithelial-mesenchymal transitions: twist in development and metastasis. Cell. 2004; 118:277–9. [PubMed: 15294153]
80. Thiery JP, Morgan M. Breast cancer progression with a Twist. Nature medicine. 2004; 10:777–8.
81. Zavadil J, Bottinger EP. TGF-beta and epithelial-to-mesenchymal transitions. Oncogene. 2005; 24:5764–74. [PubMed: 16123809]
82. Wendt MK, Smith JA, Schiemann WP. Transforming growth factor-beta-induced epithelial-mesenchymal transition facilitates epidermal growth factor-dependent breast cancer progression. Oncogene. 2010; 29:6485–98. [PubMed: 20802523]
83. Li J, Zhou BP. Activation of beta-catenin and Akt pathways by Twist are critical for the maintenance of EMT associated cancer stem cell-like characters. BMC Cancer. 2011; 11:49. [PubMed: 21284870]
84. Iliopoulos D, Polytarchou C, Hatziapostolou M, Kottakis F, Maroulakou IG, Struhl K, et al. MicroRNAs differentially regulated by Akt isoforms control EMT and stem cell renewal in cancer cells. Sci Signal. 2009; 2:ra62. [PubMed: 19825827]
85. Irie HY, Pearline RV, Grueneberg D, Hsia M, Ravichandran P, Kothari N, et al. Distinct roles of Akt1 and Akt2 in regulating cell migration and epithelial-mesenchymal transition. J Cell Biol. 2005; 171:1023–34. [PubMed: 16365168]
86. Wang YK, Zhu YL, Qiu FM, Zhang T, Chen ZG, Zheng S, et al. Activation of Akt and MAPK pathways enhances the tumorigenicity of CD133+ primary colon cancer cells. Carcinogenesis. 2010; 31:1376–80. [PubMed: 20530554]
87. Bakin AV, Tomlinson AK, Bhowmick NA, Moses HL, Arteaga CL. Phosphatidylinositol 3-kinase function is required for transforming growth factor beta-mediated epithelial to mesenchymal transition and cell migration. The Journal of biological chemistry. 2000; 275:36803–10. [PubMed: 10969078]
88. Han M, Liu M, Wang Y, Chen X, Xu J, Sun Y, et al. Antagonism of miR-21 reverses epithelial-mesenchymal transition and cancer stem cell phenotype through AKT/ERK1/2 inactivation by targeting PTEN. PLoS One. 2012; 7:e39520. [PubMed: 22761812]
89. Li Q, Qi B, Oka K, Shimakage M, Yoshioka N, Inoue H, et al. Link of a new type of apoptosis-inducing gene ASY/Nogo-B to human cancer. Oncogene. 2001; 20:3929–36. [PubMed: 11494121]
90. Kuang E, Wan Q, Li X, Xu H, Zou T, Qi Y. ER stress triggers apoptosis induced by Nogo-B/ASY overexpression. Experimental cell research. 2006; 312:1983–8. [PubMed: 16687140]
91. Oertle T, Merkler D, Schwab ME. Do cancer cells die because of Nogo-B? Oncogene. 2003; 22:1390–9. [PubMed: 12618765]

Biological significance

Our previous publication showed that NgBR is highly expressed in human breast invasive ductal carcinoma. However, the roles of NgBR and NgBR-mediated signaling pathway in breast tumor cells are still unclear. Here, we not only demonstrated that the quantitative proteomics analysis is a powerful tool to investigate the global biological function of NgBR, but also revealed that NgBR is involved in the transition of breast epithelial cells to mesenchymal stem cells, which is one of the major mechanisms involved in breast cancer metastasis. These findings provide new insights for understanding the roles of NgBR in regulating breast epithelial cell transform during the pathogenesis of breast cancer.

Highlights

- Pseudo triplex labeling approach is suitable for analysis of biological samples.
- NgBR deficiency diminishes the expression of mesenchymal cell markers.
- NgBR deficiency results in the MET of MDA-MB-231 breast tumor cells.
- NgBR deficiency prevents the TGF-β induced EMT of MCF-7 breast tumor cells.
- NgBR may play an important role in switching decision between EMT and MET.

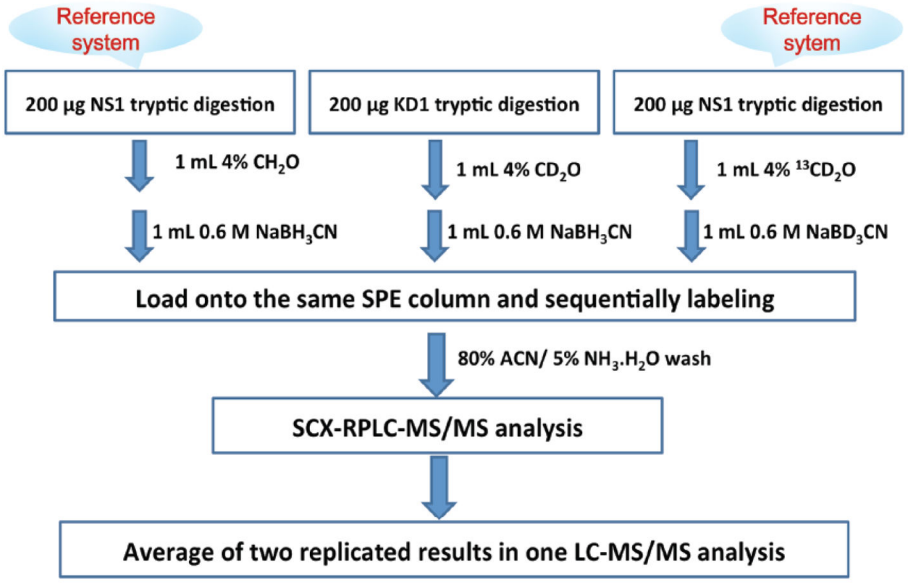

Figure 1. Flowchart of pseudo triplex labeling approach

Tryptic digests of NS control sample were loaded onto the SPE column and then flushed with the light labeling reagent. After washed, tryptic digest of NgBR knockdown sample were loaded onto the same SPE column and then were labeled with the intermediate labeling reagent. After washed, the same amount of tryptic digests of NS control sample were loaded onto the column again and labeled with the heavy labeling reagent. The labeled sample mixture was eluted with 500 µL × 2 of 80% ACN containing 5% ammonia solution and dried by the vacuum centrifugation. The lyophilized samples were first resuspended and was injected automated onto the SCX trap column. Then, a series stepwise elution with salt concentrations of 50, 100, 150, 200, 250, 300, 350, 400, 500 and 1000 mM NH_4AC (pH 2.7) was utilized to gradually elute peptides from SCX trap column to the C18 separation column. Finally, a 90 min binary RP gradient nano-RPLC MS/MS analysis was applied to separate peptides prior to mass spectrometry detection. The LTQ-Orbitrap XL mass spectrometer (Thermo Scientific, San Jose, CA, USA) was operated in a data dependent MS/MS acquisition mode. System controlling and data collection were carried out by Xcalibur software version 2.0.7 (Thermo Scientific).

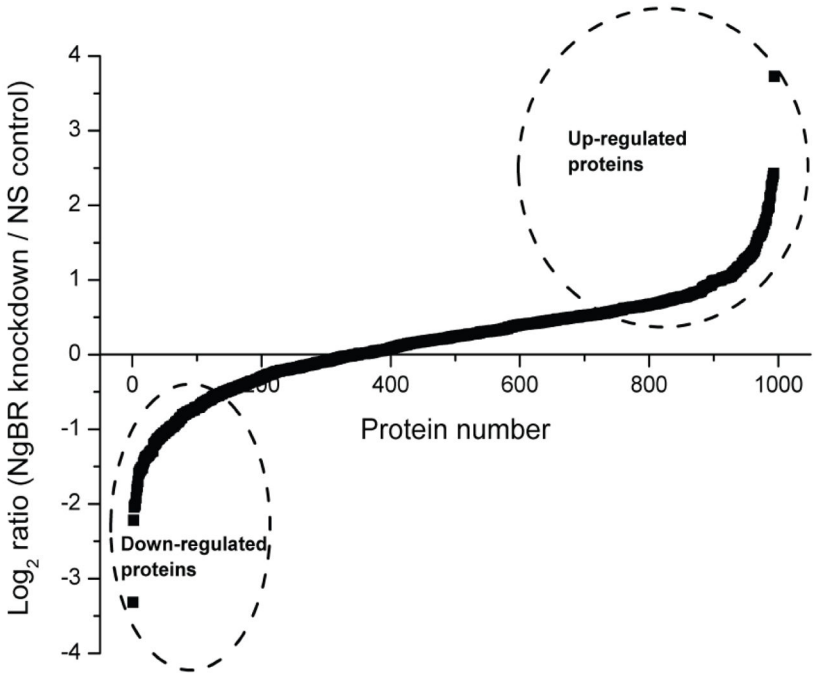

Figure 2. Log2 ratio distributions of the 994 reliable quantified proteins in both biological replicates

Among them, 248 proteins were up-regulated whereas 122 proteins were down-regulated in the NgBR knockdown versus NS control MDA-MB-231 breast cancer cells.

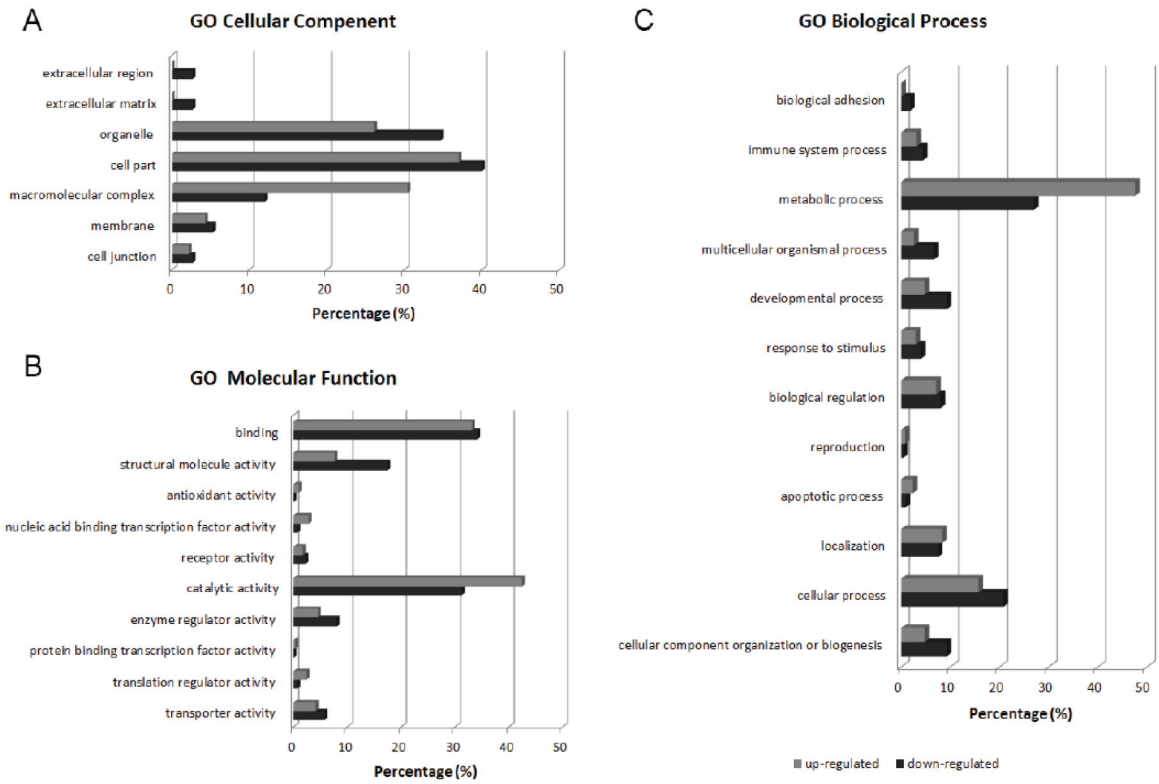

Figure 3. GO classification of the reliably quantified proteins up-and down-regulated in NgBR knockdown MDA-MB-231 cells

(A) GO cellular component, (B) GO molecular function and (C) GO biological process. Gray color bar: up-regulated proteins; Black color bar: down-regulated proteins

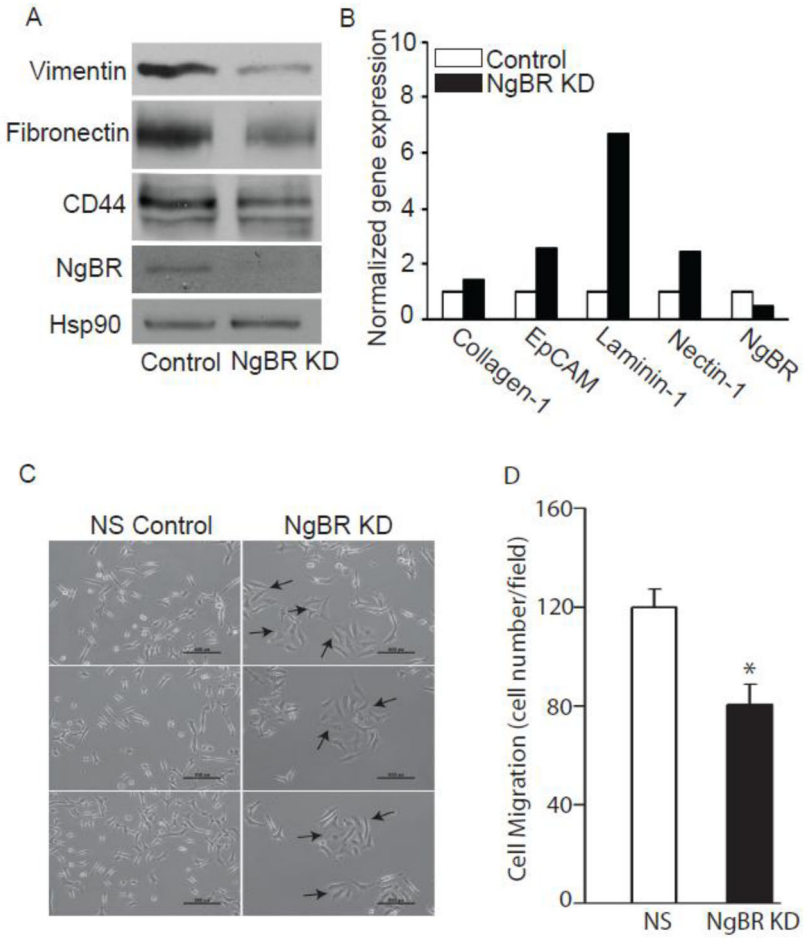

Figure 4. NgBR knockdown in MDA-MB-231 cells results in reversibility of Epithelial-Mesenchymal Transition (EMT)

(A) NgBR knockdown decreases the expression of mesenchymal markers (vimentin, S100A4 and fibronectin), and stemness indicator CD44 in MDA-MB-231 breast cancer cells. Protein changes were determined by Western blot analysis. (B) NgBR knockdown increases the expression of epithelial cell markers, collagen-1, EpCAM, Laminin-1 and nectin-1 in MDA-MB-231 breast cancer cells. Gene transcripts were determined by quantitative PCR and normalized to Beta-Actin house keeping gene. Data are presented as fold change compare to NS control group. (C) NgBR knockdown in MDA-MB-231 cells changes the cell morphology from spindle-like mesenchymal type cells to cobblestone-like epithelial appearance. Cobblestone-like epithelial cells are pointed by arrows. Cell morphology change was determined by images taken with a phase contrast inverted microscope at x 10 magnification. Scale bar = 160 μm. (D) NgBR knockdown impaired the migration of MDA-MB-231 cells. Cell migration was determined by transwell migration assay as described in the Method. * $P < 0.05$, n=4.

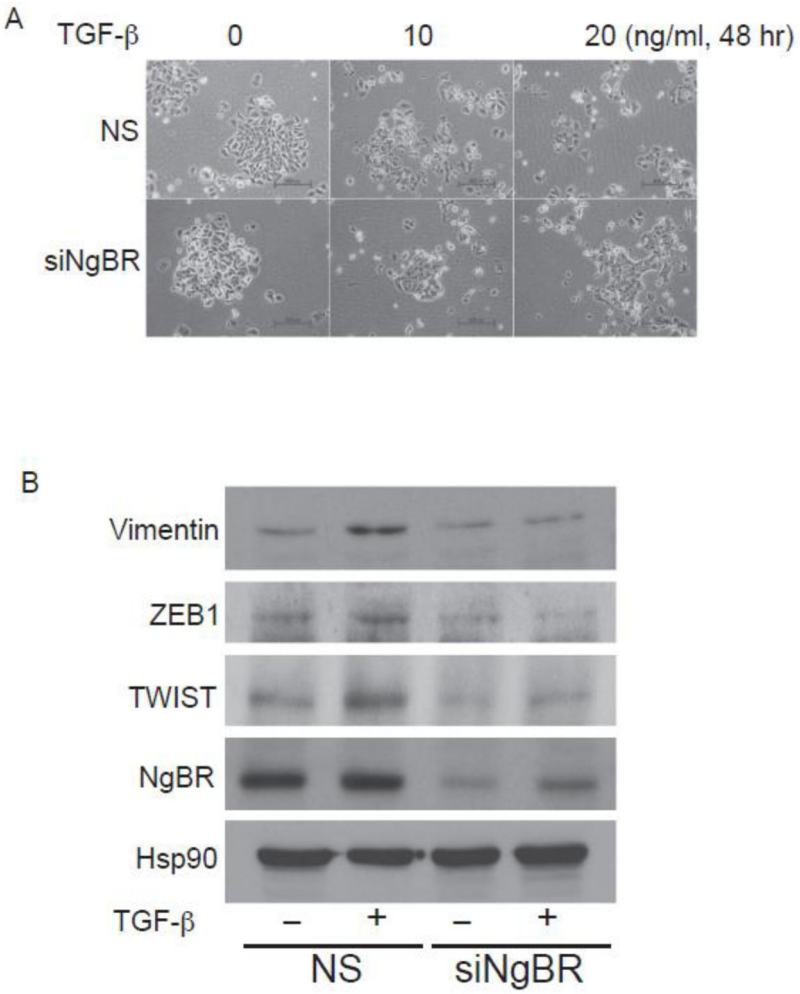

Figure 5. NgBR knockdown prevents the TGF-β induced-EMT of MCF-7 breast tumor cells

(A) NgBR knockdown in MCF-7 cells prevents the cell morphology change from cobblestone-like epithelial appearance to spindle-like mesenchymal type cells after 48 hours of TGF-β treatment at the concentration of 10 ng/ml and 20 ng/ml, respectively. Cell morphology change was determined by images taken with a phase contrast inverted microscope at x 10 magnification. Scale bar = 160 μm. (B) NgBR knockdown decreases TGF-β-induced expression of the mesenchymal marker, vimentin, and TWIST and ZEB1, transcription factors required fro EMT, in MCF-7 breast tumor cells. Protein changes were determined by Western blot analysis.

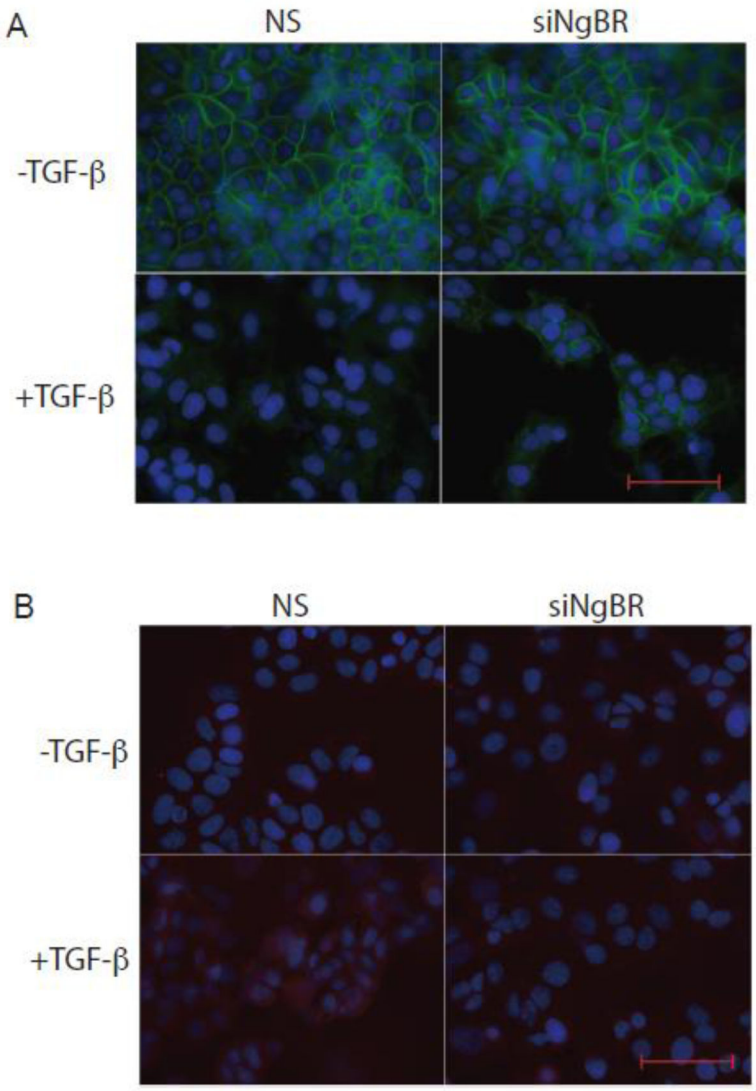

Figure 6. NgBR knockdown prevents the TGF-β induced-EMT morphology change of MCF-7 breast tumor cells

MCF-7 cells were treated with TGF-β at the concentration of 10 ng/ml for 48 hours. Images were taken with an inverted fluorescence microscope at x 20 magnification. Scale bar=200μm. (A) NgBR knockdown in MCF-7 cells prevents TGF-β-induced the loss of E-cadherin positive intercellular junction. Immunofluorescence staining of E-cadherin was performed to examine the intercellular junction of epithelial cells. (B) NgBR knockdown decreases TGF-β-induced expression of the mesenchymal marker, vimentin, in MCF-7 breast tumor cells. Vimentin positive mesenchymal cells were determined by immunofluorescence staining of vimentin.

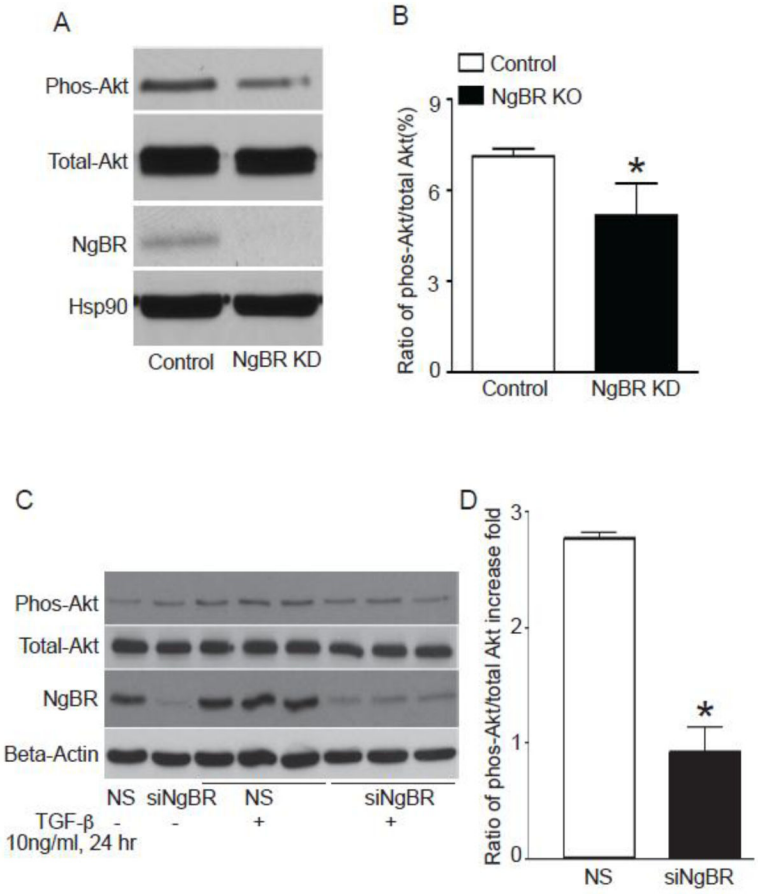

Figure 7. NgBR knockdown decreases the phosphorylation of Akt in breast tumor cells

(A) NgBR knockdown decreases the phosphorylation of Akt in MDA-MB-231 cells determined by Western blot analysis. (B) Quantitative results of phos-Akt to total Akt ratio in MDA-MB-231 cells determined by density measurement using the NIH ImageJ software. (C) NgBR knockdown decreases the TGF-β-induced phosphorylation of Akt in MCF-7 cells determined by Western blot analysis. (D) Quantitative results of phos-Akt to total Akt ratio increase fold compare to non TGF-β treatment group in MCF-7 cells determined by density measurement using the NIH ImageJ software.

Table 1

Protein down-regulated in NgBR knockdown tumor cells

Category	Accession number	Gene name	Protein Description	Protein abundance ratio	
				KD1/NS1	KD2/NS2
Extracellular markers	IPI00297160.4	CD44	cell surface glycoprotein CD44	0.180	0.189
	IPI00011302.1	CD59	cell surface glycoprotein CD59	0.393	0.698
	IPI00298851.4	CD151	cell surface glycoprotein CD151	0.312	0.309
	IPI00179700.3	HMGA1	Isoform HMG-I of High mobility group protein	0.519	0.385
Cytoskeleton proteins	IPI00418471.6	Virmentin	intermediate filament protein	0.520	0.747
	IPI00008603.1	ACTA2	aortic smooth muscle actin	0.613	0.812
	IPI00032313.1	S100A4	Calcium-binding protein S100A4	0.260	0.546
	IPI00027463.1	S100A6	Calcium-binding protein	0.524	0.461
	IPI00183695.9	S100A10	Calcium-binding protein	0.314	0.598
	IPI00013895.1	S100A11	Calcium-binding protein	0.423	0.338
	IPI00218918.5	ANXA1	Annexin A1	0.553	0.345
	IPI00418169.3	ANXA2	annexin A2 isoform 1	0.394	0.289
	IPI00024095.3	ANXA3	Annexin A3	0.393	0.239
	IPI00002459.4	ANXA6	annexin VI isoform 2	0.630	0.485
	IPI00008868.3	MAP1B	Microtubule-associated protein 1B	0.312	0.463
	IPI00302592.2	FLNA	Isoform 2 of Filamin-A	0.480	0.420
	IPI00289334.1	FLNB	Isoform 1 of Filamin-B	0.464	0.468
	IPI00178352.5	FLNC	Isoform 1 of Filamin-C	0.474	0.717
GT Pases	IPI00005719.1	RAB1A	Isoform 1 of Ras-related protein Rab-1A	0.583	0.527
	IPI00016339.4	RAB5C	Ras-related protein Rab-5C	0.583	0.427
	IPI00020436.4	RAB11B	Ras-related protein Rab-11B	0.599	0.648
	IPI00007189.1	CDC42	Isoform 1 of Cell division control protein 42 homolog	0.629	0.805
	IPI00010270.1	RAC2	Ras-related C3 botulinum toxin substrate 2	0.574	0.550
	IPI00027434.1	RHOC	Rho-related GTP-binding protein RhoC	0.646	0.694